Editors' Suggestion

Probing Magnetic Exchange Interactions with Helium

C. Trainer,[1] C. M. Yim,[1,2] C. Heil,[3] L. S. Farrar,[1] V. Tsurkan,[4,5] A. Loidl,[4] and P. Wahl[1]
[1]SUPA, School of Physics and Astronomy, University of St Andrews, North Haugh, St Andrews KY16 9SS, United Kingdom
[2]Tsung Dao Lee Institute & School of Physics and Astronomy, Shanghai Jiao Tong University, Shanghai 200240, China
[3]Institute of Theoretical and Computational Physics, Graz University of Technology, NAWI Graz, 8010 Graz, Austria
[4]Center for Electronic Correlations and Magnetism, Experimental Physics V, University of Augsburg, D-86159 Augsburg, Germany
[5]Institute of Applied Physics, MD 2028 Chisinau, Republic of Moldova

(Received 17 November 2020; revised 3 September 2021; accepted 8 September 2021; published 12 October 2021)

Controlling and sensing spin polarization of electrons forms the basis of spintronics. Here, we report a study of the effect of helium on the spin polarization of the tunneling current and magnetic contrast in spin-polarized scanning tunneling microscopy (SP STM). We show that the magnetic contrast in SP STM images recorded in the presence of helium depends sensitively on the tunneling conditions. From tunneling spectra and their variation across the atomic lattice we establish that the helium can be reversibly ejected from the tunneling junction by the tunneling electrons. The energy of the tunneling electrons required to eject the helium depends on the relative spin polarization of the tip and sample, making the microscope sensitive to the magnetic exchange interactions. We show that the time-averaged spin polarization of the tunneling current is suppressed in the presence of helium and thereby demonstrate voltage control of the spin polarization of the tunneling current across the tip-sample junction.

DOI: 10.1103/PhysRevLett.127.166803

Spintronics is based on using the electron spin for advanced functionalities, and has been a key enabler for the increase in storage density of hard disk drives over the past decades. Tunneling magnetoresistance (TMR) is at the basis of modern hard disk read heads and magnetoresistive random access memory. While reading out magnetic information using TMR is well established, controlling spin polarization and magnetization using electric fields is desirable for advanced spintronics devices such as spin transistors. Here, we investigate the influence of helium in a tunneling junction on the spin polarization (SP) of the tunneling current [Fig. 1(a)], and demonstrate voltage control of the SP. The use of probe particles (PP) in a tunneling junction [1–3], such as He here, and even scanning of a contact [4–6] enables imaging with an astonishing level of detail not accessible with a normal metal tip in tunneling. The PP acts as an atomic scale transducer which converts the Pauli repulsion between the orbitals of the PP, tip, and sample into changes in the tunneling current [3]. While scanning with a magnetic adatom in contact can lead to enhanced magnetic contrast [6], the influence of PPs on the SP is less clear. In a previous study, an increased magnetic contrast of cobalt islands on Pt(111) [7] has subsequently been attributed to the presence of hydrogen [8]. Using a PP in spin-polarized imaging promises new control over the SP. Furthermore, analogous to the PP providing information on the atomic forces in a nonmagnetic junction, for a magnetic junction it can be expected to reveal information on the magnetic exchange interactions.

We report on the effect of a PP on the SP of the tunneling current and the dependence of its binding energy on the relative magnetization of tip and sample. We have conducted spin-polarized scanning tunneling microscopy (SP STM) to determine the spin polarization and use a probe-particle model to understand the changes in the spin polarization of the tunneling current in the presence of helium. Tunneling spectra show clear signatures of the binding energy of the helium, which we find to be sensitive to the relative magnetization of tip and sample, enabling determination and imaging of the exchange interaction.

We use a low temperature Scanning Tunneling Microscope (STM) at a temperature of 4.2 K to perform SP STM measurements on a sample of iron telluride, $Fe_{1.1}Te$, in a He environment. $Fe_{1+x}Te$ exhibits for $x < 0.12$ and at temperatures below 65 K a bicollinear antiferromagnetic (AFM) order [18–20] which we use to quantify the spin polarization of the tunneling current. Samples of $Fe_{1+x}Te$ are cleaved in cryogenic vacuum [21,22]. The presence of interstitial Fe allows for *in situ* preparation of magnetic tips for SP STM [20,23]. We have admitted controlled amounts of He into the vacuum chamber, taking care to measure only with low voltages on the scan piezo to prevent arc discharges which would destroy the STM. Bias voltages V are applied to the sample with the tip at virtual ground. Differential

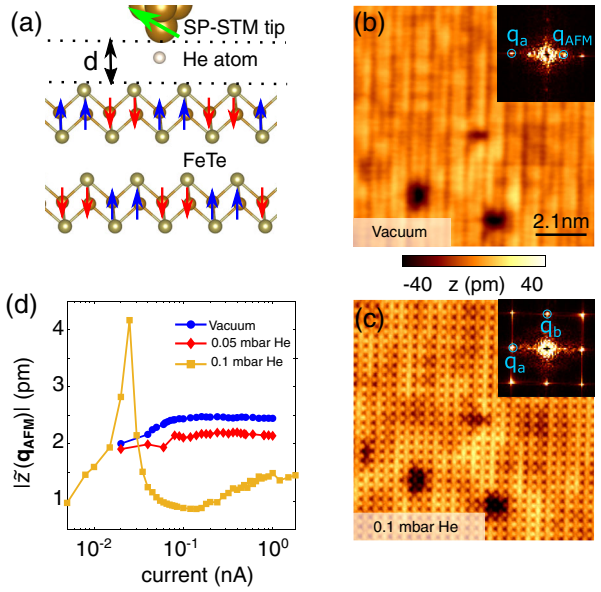

FIG. 1. (a) Schematic of the geometry of the experiment with a He atom as PP in the tunneling junction. d denotes the tip-sample distance (Sec. S2A of the Supplemental Material [9]). Magnetic moments in $Fe_{1+x}Te$ are drawn vertical for clarity, but point into the plane of the figure in reality [17]. (b) Topographic SP STM image $z(\mathbf{r})$ of $Fe_{1+x}Te$ measured in vacuum ($V = 50$ mV, $I = 100$ pA). The bicollinear AFM order of $Fe_{1+x}Te$ is seen as a stripelike modulation. Inset: Fourier transformation $|\tilde{z}(\mathbf{q})|$. (c) $z(\mathbf{r})$ image recorded with the same tip and in the same location as (b) after admission of He into the vacuum chamber at a partial pressure $p_{He} = 0.1$ mbar. The magnetic contrast is hardly visible. Inset: corresponding $|\tilde{z}(\mathbf{q})|$. (d) Amplitude $|\tilde{z}(\mathbf{q}_{AFM})|$ of the Fourier peak associated with the AFM order at different tunneling currents for a bias voltage of $V = 50$ mV in vacuum, and with $p_{He} = 0.05$ mbar and 0.1 mbar.

conductance spectra $g(V)$ were recorded using a lock-in technique with a modulation voltage V_{mod}. Tip-sample distances d are relative to the distance $d = 0$ Å where the current $I(z)$ as a function of tip height z changes its behavior from exponential vacuum tunneling (see Sec. S2A of the Supplemental Material [9]).

To model the influence of the PP on the spin polarization of the tunneling junction, we have performed density functional theory (DFT) calculations of a surface slab of FeTe with the He atom and an Fe tip, as well as of surface slabs covered with a layer of He (for details see Sec. S1A of the Supplemental Material [9]). Tip-sample distances d_{DFT} in the calculations refer to the component of the distance between the topmost Te atom and the closest tip atom in the direction normal to the surface. To simulate STM tunneling currents we employ the theory of Tersoff and Hamann [24].

The surface magnetic order of $Fe_{1+x}Te$ is observed in topographic SP STM images $z(\mathbf{r})$ as a stripelike modulation along the crystallographic a axis [Fig. 1(b)] [17,20,23,25,26]. In the Fourier transformation $\tilde{z}(\mathbf{q})$ [inset of Fig. 1(b)], the additional modulation has a wave vector of $\mathbf{q}_{AFM} = (\frac{1}{2}, 0)$, half of that of the tellurium lattice, $\mathbf{q}_a = (1, 0)$.

Following admission of He, the appearance of the surface changes dramatically. Figure. 1(c) shows a $z(\mathbf{r})$ image recorded at the same location and using the same magnetic tip and identical tunneling parameters as in Fig. 1(b) with a partial pressure $p_{He} = 0.1$ mbar. The He leads to a suppression of the magnetic contrast and an enhancement in the atomic contrast. This change is also manifested in the Fourier transformation $\tilde{z}(\mathbf{q})$ [inset of Fig. 1(c)], where peaks associated with the magnetic order at $\mathbf{q}_{AFM}$ become much weaker, while those of the crystal lattice become more intense.

In the presence of He, the magnetic contrast becomes highly sensitive to the tunneling parameters and the partial pressure p_{He}. Using the same magnetic tip, we have measured the intensity of the magnetic contrast $|\tilde{z}(\mathbf{q}_{AFM})|$ as a function of tunneling current I, and thus tip-sample distance, for fixed bias voltage $V = 50$ mV in vacuum and at two different partial pressures p_{He}. In vacuum, $|\tilde{z}(\mathbf{q}_{AFM})|$ shows only little variation with the tunneling current [Fig. 1(d)]. With $p_{He} = 0.05$ mbar, $|\tilde{z}(\mathbf{q}_{AFM})|$ becomes weaker, while the overall trend as a function of current remains largely the same. At higher $p_{He} = 0.1$ mbar, the current dependence becomes very different. $|\tilde{z}(\mathbf{q}_{AFM})|$ peaks at low current, for large tip-sample distances, drops to a minimum at $I \sim 0.1$ nA before starting to rise again with increasing current and decreasing tip-sample distance. This finding suggests a significant influence of the presence of helium on the spin polarization of the tunneling current.

In order to understand how the presence of He affects the spin polarization, we have characterized the junction in He by tunneling spectroscopy. Figure 2(a) shows $g(V)$ spectra for different tip-sample distances d at $p_{He} = 0.1$ mbar and a typical spectrum recorded in vacuum. The $g(V)$ spectrum recorded in vacuum is independent of d. When He is added, the spectrum develops a d dependence and a pronounced gaplike feature whose width varies between 20 and 135 mV for d between 2.6 and 4.6 Å (see Fig. S6 of the Supplemental Material [9]). For $d \geq 4.6$ Å, the spectrum resembles that obtained in vacuum. The gap size is largest for $d \sim 4.1$ Å where the gap edge develops peaklike features.

Similar spectroscopic gaps have been observed using H_2 as PP and were attributed to inelastic excitations of internal degrees of freedom of H_2 [27], or bouncing of the H_2 in the tunneling junction [28]. Here, excitations due to internal degrees of freedom can be excluded as He is monatomic. Similarly, a vibrational mode of the He atom normal to the surface can be ruled out as the characteristic energy is expected to increase with decreasing d (see Sec. S1A of the Supplemental Material [9]), opposite from what we observe here.

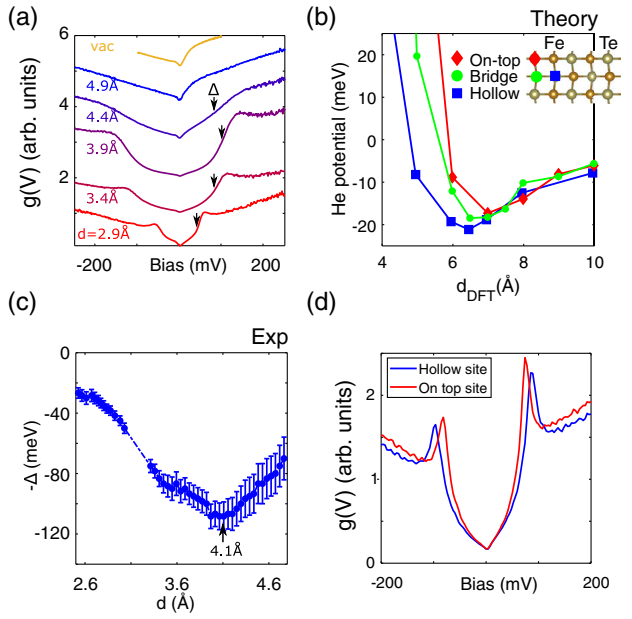

FIG. 2. Spectroscopy in He at $p_{\mathrm{He}} = 0.1$ mbar. (a) Differential conductance spectra $g(V)$ ($V = 50$ mV, $I = 80$ pA, $V_{\mathrm{mod}} = 5$ mV) recorded at different d in the presence of He. A $g(V)$ spectrum taken in vacuum (yellow) is also shown ($V = 100$ mV, $I = 300$ pA, $V_{\mathrm{mod}} = 1$ mV). Spectra are vertically offset for clarity and normalized at $V = 250$ mV. (b) DFT calculation of the trapping potential for the He atom in the junction for different adsorption sites. (c) The gap size $\Delta(d)$, plotted as $-\Delta(d)$, extracted from $g(V)$ spectra (defined as the inflection point at the gap edge) as a function of d. $\Delta(d)$ exhibits a similar functional form as the potential of the He atom found in the DFT calculation in (b). (d) $g(V)$ spectra recorded with the tip positioned above the hollow (blue) and on-top site (red) showing a larger gap for the hollow site ($V = 20$ mV, $I = 1$ nA, $V_{\mathrm{mod}} = 3.5$ mV).

We interpret the gap as the excitation gap for ejecting the He from the tunneling junction. To support this interpretation, we have modeled the trapping energy of a He atom in a junction consisting of an Fe tip and a FeTe surface in a DFT calculation. By changing the separation d_{DFT} of the tip and the sample we have mapped out the potential of the He atom in the hollow, on-top, and bridge sites, Fig. 2(b). The curves resemble a Lennard-Jones potential with the preferred site being the hollow site.

We show in Fig. 2(c) the magnitude of the gap Δ, defined as the inflection point of $g(V)$ at the gap edge, as a function of d [plotted as $-\Delta(d)$]. The qualitative shape is in good agreement with the potential energy of the He atom obtained from DFT calculations. The higher conductance once the He atom is ejected for $|V| > \Delta$ can be attributed to a larger overlap of the wave functions of tip and sample in the absence of He as well as contributions from inelastic processes.

Spectra acquired at the hollow and on-top sites [Fig. 2(d)] show a difference in Δ of 10 mV confirming this interpretation. Δ obtained from the $g(V)$ spectra is about a factor of 4 larger than the binding energy obtained from the DFT calculations. This difference can be explained by a lack of knowledge of the precise structure of the tip apex [29]. Measurements with different tips reproduce the d dependence of Δ but with variations in shape and slight changes in the magnitude of Δ (see Fig. S7 of the Supplemental Material [9]).

We can use this information about the binding energy of He in the different sites to model the influence of the PP on the magnetic imaging. Experimentally, we observe that the magnetic contrast $|\tilde{z}(\mathbf{q}_{\mathrm{AFM}})|$ exhibits a strong dependence on bias voltage V and d. As a function of d, the magnetic contrast $|\tilde{z}(\mathbf{q}_{\mathrm{AFM}})|$ shows a sharp dip at $d \sim 3.7$ Å and a peak at $d \sim 4.5$ Å when imaged with $V = 75$ mV, whereas for larger V both features become less pronounced [Fig. 3(c)] until the contrast becomes independent of d as for vacuum tunneling (see, e.g., the curve for $V = 200$ mV). In the following, we will introduce a model to explain (i) the suppression of spin polarization for small d and bias voltages V and (ii) the enhanced magnetic contrast at larger d.

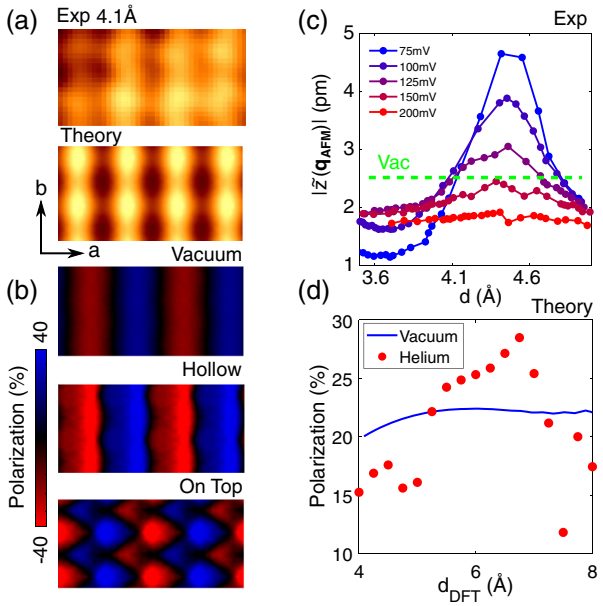

FIG. 3. (a) $z(\mathbf{r})$ image for $d = 4.1$ Å ($V = 50$ mV, $I = 30$ pA) and the simulated topography for $d_{\mathrm{DFT}} = 7.6$ Å for comparison. (b) calculated SP at the same d_{DFT} for vacuum tunneling and for a layer of He in the hollow and the on-top sites. The largest magnetic contrast is observed for He in the hollow site. (c) Amplitude $|\tilde{z}(\mathbf{q}_{\mathrm{AFM}})|$ of the magnetic contrast as a function of d and for a range of voltages V. The green dashed line represents the value for vacuum tunneling. (d) The SP P extracted from the amplitude of the magnetic contrast in the simulated images. Red points are extracted from our model accounting for the He atom probing different sites during the measurement (for details see Sec. S1B of the Supplemental Material [9]). The blue curve is the amplitude of the magnetic contrast for a vacuum junction.

While in our experiment we expect the PP to follow the STM tip, we have simulated STM images to approximate the imaging process in a slab calculation with He atoms placed at different adsorption sites on the surface. These calculations reproduce similar contrast as observed in the experimental images though with no significant suppression of the magnetic contrast. Figure 3(a) shows a simulated image for He in the hollow site, showing excellent agreement with the image obtained from experiment at $d = 4.1$ Å. SP images are obtained from the spin-resolved densities of states $\rho_\uparrow(\mathbf{r})$ and $\rho_\downarrow(\mathbf{r})$ to determine $P = [(\rho_\uparrow - \rho_\downarrow)/(\rho_\uparrow + \rho_\downarrow)]$ at a height d_{DFT} above the surface [Fig. 3(b)]. From the calculations and with a He atom in the hollow site, we find an overall increase in the spin polarization of up to ~30% compared to without He, while He in the on-top position leads to a more complex pattern. We attribute these results to the effect of Pauli repulsion reducing the density of states above the He atom (see Sec. S1A of the Supplemental Material [9]). When the He is at a Te site it suppresses tunneling to the Te p orbitals more than tunneling to the spin-polarized Fe d states. This results in a phase shift of the magnetic order in the simulated images dependent on the adsorption site of the He [see Fig. 3(b) and Fig. S2 of the Supplemental Material [9]]. The suppression we observe experimentally suggests that the He atom does not stay in the same site during imaging, but probes a distribution of sites closest to the tip. To model this imaging process we account for the potential energy landscape of the He atom in the presence of the tip, using the calculated potential energy curves [Fig. 2(b)]. We estimate the binding energy of the He atom at each site for a given tip position and then combine the calculated SP images weighting their contributions using a Boltzmann factor. The resultant behavior of the SP as a function of d_{DFT} obtained from the calculation [Fig. 3(d)] reproduces the suppression in SP seen experimentally for small d [Fig. 3(c)] and also exhibits an increase for larger d when the He atom is trapped mostly in the hollow site. The change in preferred adsorption site is accompanied by a phase shift which is also seen experimentally (see Fig. S3 of the Supplemental Material [9]).

We conclude that the suppression of spin polarization for small d is due to the He atom hopping between neighboring sites, scrambling the information of the spin polarization over the time of the measurement. However, the increase in SP seen at some values of d obtained from the model is significantly lower compared with that seen experimentally: in the experiment, we observe an increase in magnetic contrast by almost a factor of 2, whereas the calculation can only account for an increase by about 33% compared with vacuum tunneling. Therefore, the enhanced magnetic contrast requires a different mechanism.

To better understand the strong increase in magnetic contrast at $d \approx 4.5$ Å and $V = 75$ mV we spatially map the binding energy Δ at the atomic scale from a spectroscopic map $g(\mathbf{r}, V)$. In a $\Delta(\mathbf{r})$ map [Fig. 4(a)] extracted from a $g(\mathbf{r}, V)$ map with He in the tunneling junction, one can clearly see the variation of Δ between the on-top, hollow, and bridge sites.

The map also reveals that the binding energy of the He atom depends on the relative orientation of the tip and sample magnetization. Figure 4(b) shows that Δ varies between otherwise equivalent hollow sites with parallel and antiparallel orientation of the magnetizations of the tip and sample by about 3 meV. The binding energy of the He is thus sensitive to the exchange interaction between the tip and the sample, providing a new way to image the magnetic order of the surface: By adjusting the bias voltage to between the energies which eject the He from the two hollow sites with opposite magnetization, here about 75 mV, the He is ejected for one relative configuration, but not the other leading to a huge amplification in the magnetic contrast.

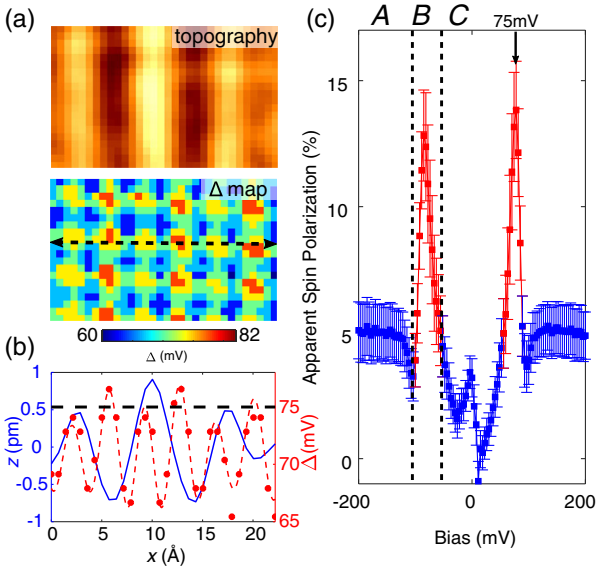

FIG. 4. (a) Topography $z(\mathbf{r})$ ($V = 200$ mV, $I = 1$ nA) and spatial map of binding energy $\Delta(\mathbf{r})$ of the He atom extracted from a spectroscopic map $g(\mathbf{r}, V)$ ($V = 20$ mV, $I = 1$ nA, $V_{\mathrm{mod}} = 3.5$ mV) acquired with a setpoint at which the magnetic contrast is not visible in the topography. The $\Delta(\mathbf{r})$ map shows clear variations between different atomic sites. (b) Average profile from $z(\mathbf{r})$ (blue curve) and along the dashed line from $\Delta(\mathbf{r})$ (red curve) in (a). Besides the difference in Δ between the hollow and on-top sites, a ~3 mV modulation is observed between hollow sites with different relative magnetization of tip and sample. (c) The apparent SP of the tunnel junction extracted from the $g(\mathbf{r}, V)$ map. Blue points show true spin polarization, red points show enhancement due to the exchange interaction, leading to a giant apparent SP. There are three regimes: A, He is ejected from the junction; B, He is trapped only at some sites and for one relative magnetic configuration of tip and sample; and C, He remains always in the junction.

We can confirm this picture by extracting the apparent SP from the $g(\mathbf{r}, V)$ map [Fig. 4(c)], $P(V) = [g_{\uparrow\uparrow}(V) - g_{\uparrow\downarrow}(V)]/[g_{\uparrow\uparrow}(V) + g_{\uparrow\downarrow}(V)] = [|\tilde{g}(V, \mathbf{q}_{\mathrm{AFM}})|]/[\tilde{g}(V, \mathbf{q} = 0)]$ [30,31]. For $|V| \gg \Delta$ (region A) the He atom is ejected from the junction and the SP is comparable to that seen in vacuum tunneling. A huge apparent enhancement of the SP is found for $|V| \sim \Delta$ (region B) when the difference in the binding energy of He for different relative magnetization of the tip and sample straddles the bias voltage V, leading to He being ejected for one relative configuration, but not for the other. For $|V| \ll \Delta$, there is a strong suppression of the SP (region C) due to the presence of He.

The suppression we observe in region C also explains why in all but one [32] of the previous studies of FeTe by STM, signatures of the bicollinear magnetic order have been observed [20,23,25,26,33]. The experiment in Ref. [32] was conducted in He, likely explaining why no magnetic order was observed.

We show that the time-averaged spin polarization of the tunneling current can be suppressed by the presence of helium in the junction due to the dynamics of the probe particle. Using the bias voltage, the PP can be ejected in a controlled way from the tunneling junction, thus enabling control of the average spin polarization of the current. We further demonstrate that the probe particle can be used to determine exchange interactions between the tip and sample in a scanning tunneling microscope, complementing direct force measurements [34].

The supporting data for this article are openly available from [35].

We gratefully acknowledge useful discussions with Pavel Jelinek. C. T. and P. W. acknowledge support from EPSRC (EP/R031924/1) and C. M. Y. and L. S. F. from EP/S005005/1. C. H. acknowledges support by the Austrian Science Fund (FWF) Project No. P32144-N36 and the VSC-4 of the Vienna University of Technology and V. T. by ANCD 20.80009.5007.19 (Moldova). The work was partially supported by the Deutsche Forschungsgemeinschaft (DFG) through Transregional Research Collaboration TRR 80 (Augsburg, Munich, and Stuttgart).

[1] C. Wagner and R. Temirov, Prog. Surf. Sci. **90**, 194 (2015).
[2] R. Temirov, S. Soubatch, O. Neucheva, A. C. Lassise, and F. S. Tautz, New J. Phys. **10**, 053012 (2008).
[3] C. Weiss, C. Wagner, C. Kleimann, M. Rohlfing, F. S. Tautz, and R. Temirov, Phys. Rev. Lett. **105**, 086103 (2010).
[4] Y. H. Zhang, P. Wahl, and K. Kern, Nano Lett. **11**, 3838 (2011).
[5] Y.-H. Zhang, P. Wahl, and K. Kern, Phys. Rev. B **87**, 205417 (2013).
[6] S. Ouazi, A. Kubetzka, K. von Bergmann, and R. Wiesendanger, Phys. Rev. Lett. **112**, 076102 (2014).
[7] S. Rusponi, N. Weiss, T. Cren, M. Epple, and H. Brune, Appl. Phys. Lett. **87**, 162514 (2005).
[8] W. A. Hofer, K. Palotás, S. Rusponi, T. Cren, and H. Brune, Phys. Rev. Lett. **100**, 026806 (2008).
[9] See Supplemental Material at http://link.aps.org/supplemental/10.1103/PhysRevLett.127.166803 for details on theoretical modelling and additional experimental data and methods, which includes Refs. [10–16].
[10] P. Giannozzi *et al.*, J. Phys. Condens. Matter **21**, 395502 (2009).
[11] D. R. Hamann, Phys. Rev. B **88**, 085117 (2013).
[12] J. P. Perdew, K. Burke, and M. Ernzerhof, Phys. Rev. Lett. **77**, 3865 (1996).
[13] G. Kresse and D. Joubert, Phys. Rev. B **59**, 1758 (1999).
[14] M. Methfessel and A. T. Paxton, Phys. Rev. B **40**, 3616 (1989).
[15] H. J. Monkhorst and J. D. Pack, Phys. Rev. B **13**, 5188 (1976).
[16] S. Li, C. de la Cruz, Q. Huang, Y. Chen, J. W. Lynn, J. Hu, Y.-L. Huang, F.-C. Hsu, K.-W. Yeh, M.-K. Wu, and P. Dai, Phys. Rev. B **79**, 054503 (2009).
[17] C. Trainer, M. Songvilay, N. Qureshi, A. Stunault, C. M. Yim, E. E. Rodriguez, C. Heil, V. Tsurkan, M. A. Green, A. Loidl, P. Wahl, and C. Stock, Phys. Rev. B **103**, 024406 (2021).
[18] C. Koz, S. Rößler, A. A. Tsirlin, S. Wirth, and U. Schwarz, Phys. Rev. B **88**, 094509 (2013).
[19] W. Bao, Y. Qiu, Q. Huang, M. A. Green, P. Zajdel, M. R. Fitzsimmons, M. Zhernenkov, S. Chang, M. Fang, B. Qian, E. K. Vehstedt, J. Yang, H. M. Pham, L. Spinu, and Z. Q. Mao, Phys. Rev. Lett. **102**, 247001 (2009).
[20] M. Enayat, Z. Sun, U. R. Singh, R. Aluru, S. Schmaus, A. Yaresko, Y. Liu, C. Lin, V. Tsurkan, A. Loidl, J. Deisenhofer, and P. Wahl, Science **345**, 653 (2014).
[21] S. C. White, U. R. Singh, and P. Wahl, Rev. Sci. Instrum. **82**, 113708 (2011).
[22] C. Trainer, C. M. Yim, M. McLaren, and P. Wahl, Rev. Sci. Instrum. **88**, 093705 (2017).
[23] U. R. Singh, R. Aluru, Y. Liu, C. Lin, and P. Wahl, Phys. Rev. B **91**, 161111(R) (2015).
[24] J. Tersoff and D. R. Hamann, Phys. Rev. B **31**, 805 (1985).
[25] T. Hänke, U. R. Singh, L. Cornils, S. Manna, A. Kamlapure, M. Bremholm, E. M. J. Hedegaard, B. B. Iversen, P. Hofmann, J. Hu, Z. Mao, J. Wiebe, and R. Wiesendanger, Nat. Commun. **8**, 13939 (2017).
[26] C. Trainer, C. M. Yim, C. Heil, F. Giustino, D. Croitori, V. Tsurkan, A. Loidl, E. E. Rodriguez, C. Stock, and P. Wahl, Sci. Adv. **5**, eaav3478 (2019).
[27] J. A. Gupta, C. P. Lutz, A. J. Heinrich, and D. M. Eigler, Phys. Rev. B **71**, 115416 (2005).
[28] S. Li, A. Yu, F. Toledo, Z. Han, H. Wang, H. Y. He, R. Wu, and W. Ho, Phys. Rev. Lett. **111**, 146102 (2013).
[29] X. Bouju, C. Girard, H. Tang, C. Joachim, and L. Pizzagalli, Phys. Rev. B **55**, 16498 (1997).
[30] M. Bode, Rep. Prog. Phys. **66**, 523 (2003).
[31] R. Wiesendanger, Rev. Mod. Phys. **81**, 1495 (2009).

[32] T. Machida, K. Kogure, T. Kato, H. Nakamura, H. Takeya, T. Mochiku, S. Ooi, Y. Mizuguchi, Y. Takano, K. Hirata, and H. Sakata, J. Phys. Soc. Jpn. **81**, 074714 (2012).

[33] W. Li, W.-G. Yin, L. Wang, K. He, X. Ma, Q.-K. Xue, and X. Chen, Phys. Rev. B **93**, 041101 (2016).

[34] U. Kaiser, A. Schwarz, and R. Wiesendanger, Nature (London) **446**, 522 (2007).

[35] C. Trainer *et al.*, Probing magnetic exchange interactions with helium (dataset) (2021), https://doi.org/10.17630/49909dde-e576-4f1a-92a3-a91e5d035db1.